Soft Matter

Accepted Manuscript

ROYAL SOCIETY OF CHEMISTRY

www.rsc.org/softmatter

Journal Name

RSCPublishing

ARTICLE

Thermally-induced release from polymeric microparticles with liquid core: the mechanism

Cite this: DOI: 10.1039/xoxxoooooox

Alexandra Latnikova[a]*, Arda Yildirim[a]

Received ooth January 2012,
Accepted ooth January 2012

DOI: 10.1039/xoxxoooooox

www.rsc.org/

Herein we demonstrate, how the volatility of a liquid can be manipulated by enclosing microdroplets of this liquid into thin polymeric shells. In this way, composite core-shell microparticles consisting of 80 wt.% of a liquid core material and 20 wt.% of a polymer can be made 150°C more stable than the individual core component. The thermal stability of the composite microparticles is found to be determined by the boiling point of the core material and the average particle size, while the role of the particle shell thickness is much less relevant. Two mechanisms responsible for the release of the core material from the microparticles at elevated temperatures were resolved: (1) thermally-induced degradation of the shell and (2) diffusion of the core material through the polymeric shell boosted by the increased inner pressure.

Introduction

Today, we hear about newly designed materials daily, polymers undoubtedly being one of the material classes, which develop most rapidly. Very often, in order to achieve desired properties, polymers are used in combination with a number of additives, which basically carry the functionalities that cannot be provided by the polymer alone.

Being the key factor determining the final composite functionality, polymer additives became a special, highly versatile branch of the material science. As the result, the structure of these additives at both micro- and nanoscale becomes more and more elaborate. Thus, application of composite micro- and even nanoparticles with core-shell morphology already became a common practice. For many novel applications, in order to achieve the desired functionality it is important to preserve the core of the particles in the liquid state (at least until the moment its release is triggered). These novel materials include self-healing[1-3] and self-lubricating composites,[4] antifouling coatings,[5] thermal energy storage materials,[6] wound dressings,[7] electrophoretic displays,[8] smart thermo-chromic windows,[9] packaging materials with storage conditions indicators[10] and many more.

Extrusion is still one of the most conventional ways to process polymers and polymer composites. Since extrusion generally implies application of the temperatures above at least 100°C, it is essential to know about the stability of the additives at elevated temperatures. Moreover, it would be very useful to be able to tailor the thermal stability according to the application. For that, however, one should be aware of the thermal decomposition mechanisms of the additives represented by micro- and nanoparticles with the complex morphology.

Bryant figured out three general mechanisms possibly responsible for the heat-induced damage of composite microparticles: (i) shell rupture due to the increased internal pressure, (ii) diffusion of the core material through the microparticle shell; and (iii) thermal degradation of the wall, followed by the release of the core material.[11] Unfortunately, no systematic studies, which would either confirm or contradict these statements, could be found in the literature. The thermal stability has been eventually estimated for different core-shell particles together with other properties, but apart from the very few cases, never became one of the main goals of an investigation. The efforts were more focused on changing[12-15] or modifying[11, 16, 17] the shell material in order to achieve better thermal stability, and there were no investigations of the mechanisms responsible for the phenomena. Only some

studies[18] dealt with the influence of the particles' size and the core content on the thermal stability of the composite microparticles with a liquid core.

It is complicated to speak about the general stability of core-shell particles, since the degradation mechanisms can vary significantly depending on the architecture and composition. Therefore, we decided to start with studying a model system consisting of the liquid hydrocarbon core and the solid shell made of highly cross-linked polymer, which can be used as the basis for the prediction of the "real" systems behaviour.

The questions to be answered were how the parameters, such as core type, particle size and shell thickness influence the thermal stability of the microobjects. Simply put, what can happen when one starts heating microparticles with complex morphology? Using TGA as the main method, we figured out few surprising peculiarities that allowed us drawing the mechanisms responsible for the objects' thermal instability, which can be the key limiting factor for the application of microparticles as a part of a polymer composite.

Experimental

Materials

Poly[(phenyl isocyanate)-*co*-formaldehyde], average M_n ~400 (cas. 9016-87-9) further referred as "isocyanate prepolymer", cyclooctane (CO) of ≥99% purity, tetradecane (TD) of ≥99.0% purity, glycerol (ACS reagent, ≥99.5%), 1,4-Diazabicyclo[2.2.2]octane (DABCO) of ≥99% purity, anhydrous ethyl acetate 99.8% and PVA (Mowiol 4-88, M_w ~31,000) were received from Sigma. N-Heptane (N-Hep) 99% "for synthesis" and N-Nonane (N-Non) "for synthesis" were received from AppliChem and Merck, correspondingly. All chemicals were used as-received without further purification. Distilled water was used for the synthesis.

Preparation of core-shell particles with liquid hydrocarbon core:

X g of isocyanate prepolymer , Y g of core material and Z g of co-solvent (ethyl acetate) were mixed together to obtain a clear homogeneous solution (see Table 1 for the exact amounts). The amount of co-solvent in each case is only slightly (0,1-0,3 g) above the minimum amount necessary to obtain a homogeneous solution (isocyanate prepolymer and hydrocarbons are not miscible). The resulting oil phase (OP) was immediately added to 20 g of water phase 1 (WP1) consisting of aqueous PVA solution (0,5 wt.%) saturated with ethyl acetate. OP was dispersed in WP1 with high-shear mixer (U-Turrax) by stirring at 3000, 5000 or 11000 rpm for one minute (see Table 1). Then 20 g of water phase 2 (WP2) containing 4 g glycerol, 0,5 g DABCO and 15,5 g water was added to the emulsion. The resulting emulsion was placed in an open reactor at the magnetic stirrer and heated up to 75°C at 500 rpm stirring. After 2 hours the heating was stopped, the vessel was closed and the reaction mixture was kept stirred for 3 days in order to achieve high conversion of isocyanate prepolymer. The particles were washed by centrifugation at 5000 rpm followed by re-dispersion in water for 3 times. Finally, the cake of particles was separated, spread on a glass surface (ca. 1 mm thick layer) and dried overnight at room temperature and ambient humidity.

Table 1 Preparation conditions and some properties of the resulting microparticles. X = mass of isocyanate prepolymer, Y = mass of core material, Z = mass of ethyl acetate, MS = mixing speed, Tc is the temperature corresponding to the first maximum of the derivative weight loss, Pc is the inner pressure calculated according to the Antoine equation, Dmax is the diameter corresponding to the maximum on the size distribution.

Sample name	X, g	Y, g	Z, g	MS, 10^3 rpm	T_c,° C	P_c, Bar	D_{max}, µm
20_CO	0,5	CO, 2.1	1,7	11	254	7,6	3,1
30_CO	0,8	CO, 1.8	1,7	11	266	9,3	3,5
40_CO	1	CO, 1.6	1,7	11	268	9,5	3,5
50_CO	1,3	CO, 1.3	1,7	11	272	10,1	3,4
60_CO	1,5	CO, 1.1	1,7	11	259	8,4	3,8
70_CO	1,8	CO, 0.8	1,7	11	267	9,4	3,5
PU100	2,6	0	1,7	11	---	---	3,2
20_CO_B	0,5	CO, 2.1	1,7	5	284	11,9	11,8
20_CO_BB	0,5	CO, 2.1	1,7	3	292	13,2	20,7
30_He	0,8	N-Hep, 1.8	3,5	11	175	6,3	4,3
30_CO	0,8	CO, 1.8	1,7	11	266	9,3	3,5
30_No	0,8	N-Non, 1.8	3,5	11	245	7,3	4,2
30_TD	0,8	TD, 1.8	3,8	11	308	3	2,7

Characterization methods

Thermo gravimetric analysis (TGA)

Thermo gravimetric analysis was carried out on a TA Instruments Thermo gravimetric Analyzer (TGA Q500) with the heating rate of 10 K min^{-1} under nitrogen atmosphere. The weight of each sample did not exceed 7 mg. Each measurement was made at least 3 times. The graphs shown in the manuscript are representative.

In order to achieve good reproducibility of the results (which implies that samples from different batches show the same thermal behavior with ±5°C precision), special care during sample preparation has to be taken. Thus, the powders have to be handled in such a way that no core-shell particles are mechanically damaged (in this case an additional weight loss step corresponding to the evaporation of the pure core component appears). Moreover, PVA has to be washed away thoroughly; otherwise it works as a glue between the microparticles. As the result, such samples demonstrate higher thermal stability (the reproducibility is very poor, though) than the carefully washed ones.

Optical microscopy

Optical microscope imaging was performed on Axioscope 2 from ZEISS in the transmission mode.

Fourier transform infrared (FTIR) spectroscopy

FTIR measurements were carried out with a Thermo Nicolet NEXUS 470 FTIR spectrometer with DTGS/KBr detector equipped with total attenuated reflectance accessory with germanium crystal. Automatic atmosphere correction has been performed for each measurement. Spectra were recorded at

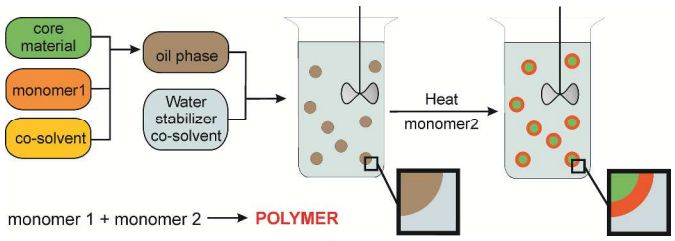

Fig. 1. Schematic representation of the microparticles' preparation. Phase separation and interfacial polymerization happen simultaneously.

room temperature between 500 and 4000 cm-1 with 2 cm-1 resolution.

PARTICLE SIZE DISTRIBUTION MEASUREMENTS

The LS 13 320 SW laser diffraction particle size analyzer from Beckman Coulter, which applies both, Mie and Fraunhofer theories of light scattering, has been utilized.

Results

The process of core-shell particles preparation (fig. 1) combines *interfacial polymerization* and *solvent evaporation induced phase separation* processes. Combination of the two processes in one ensures formation of the core-shell microparticles with the core entirely consisted of the hydrocarbon ("core material" in fig. 1), which would not be possible if solvent evaporation would not be employed. See SI for more details.

The process of particle formation can be described as follows. At the first step, O/W emulsion is formed. The oil phase (OP) contains the core material, the oil-soluble reactive monomer (isocyanante prepolymer) and the co-solvent (ethyl acetate). The water phase (WP1) contains water saturated with co-solvent and the emulsion stabilizer. Since the amount of the co-solvent in the OP is very close to the miscibility limit, while the solubility of the co-solvent in water is considerable (ca. 8 g in 100 ml of water), it is important to use the continuous phase (WP1) saturated with the co-solvent in order to avoid the phase separation in the OP already at this stage.

Water phase 2 (WP2) consists of the second reactive monomer (glycerol) and the reaction catalyst (DABCO) dissolved in water. It is added once the emulsion is formed. Presumably, a part of the co-solvent from the OP diffuses into the continuous phase at this step resulting in the beginning of the phase separation within each oil droplet. Simultaneously, polymerization reaction starts (fig. SI-1). Heating the emulsion in an open vessel allows evaporation of co-solvent and simultaneously accelerates the polymerization reaction. Evaporation of ethyl acetate from the aqueous phase (ethyl acetate forms an azeotrope with water with B_p of 70.4°C) leads to the gradual diffusion of the co-solvent from the oil phase resulting in the phase separation within each oil droplet. Being more polar than the core material, (partially polymerized) isocyanate prepolymer concentrates at the periphery of each droplet, while the core material concentrates around the centre. In 2 hours most of the co-solvent is evaporated, while the polymerization reaction has proceeded to a certain extent. During the following hours, polymerization reaction completes.

The kinetics of the polymerization reaction is controlled by the diffusion of the complementary water-soluble monomer(s) through the nascent polymeric shell formed at the initial stages of the reaction. It is well known that, in case of O/W-type systems, polymerization often happens at the inner side of the shell.[19] Consequently, the reactive species and the catalyst molecules dissolved in the continuous phase have to penetrate the polymeric membrane and diffuse towards the center of the droplet in order to take part in the polymerization reaction. The kinetics of the reaction should be, therefore, determined 1) by the partition coefficients of the reactive species and the catalyst between oil and water phases and 2) by the size of the oil droplets (since the shell thickness is proportional to the droplet radius when the composition is fixed). Indeed, we found that polymerization is almost completed after 24 hours in smaller particles (prepared at 11000 rpm stirring), while in the case of the bigger particles with the same composition (prepared at 3000 rpm stirring) it required at least 3 days to do so. Some post-heating might be useful to accelerate the process.

It was interesting to know, how the composition (in terms of the core material and core/shell ratio) and the size of the particles influence their thermal stability. In order to reveal the trends, one parameter has been varied in each experimental series while the others were fixed. The varied parameters included:

- Core material
- Core/shell ratio
- Particle size

The other synthesis conditions including the concentrations of glycerol and catalyst, reactor volume and geometry were kept the same in all the experiments. Below, the influence of each parameter will be discussed separately.

Core material

Four representatives of the family of aliphatic hydrocarbons were chosen as model liquid core materials: N-heptane (N-Hep, b.p. 98°C), cyclooctane (CO, b.p. 151°C), N-nonane (N-Non, b.p. 151°C) and tetradecane (TD, mixture of isomers, b.p. 253-257°C). Hydrocarbons were selected for having similar phase separation behaviour and, presumably, affinity to the polymeric shell material. In this way, any possible specific interactions between core and shell materials (presumably influencing the permeability and/or elasticity of the shell) can be omitted in the discussion.

The preparation of each type of the particles with the liquid core was performed in the same manner, all reaction conditions (except for the amounts of the co-solvent added) were kept identical in this experimental series. Hence, we expected to obtain four types of particles, which would differ only in their core material, while all the other parameters would be the same.

In the case of polyurethane/urea type of polymers, the progress of the polymerization reaction is relatively easy to follow by FT-IR spectroscopy (fig. 2). The absorption peak at ~2275 cm^{-1} typical for unreacted isocyanate groups, is well isolated from

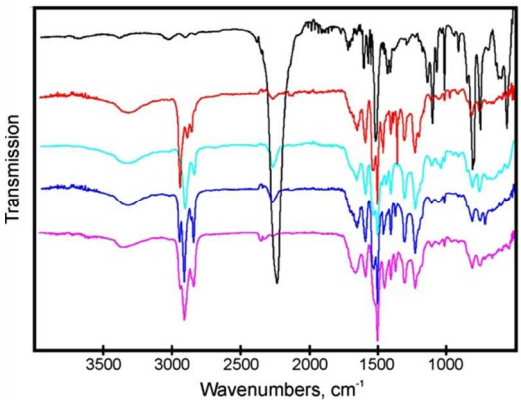

Fig. 2. FTIR spectra of the isocyanate prepolymer and the resulting samples. From top to down: Isocyanate prepolymer, N-Hep, CO, N-Non, TD. The spectra are normalized to the peak corresponding to the C-C stretching in the benzene ring (1510 cm-1).

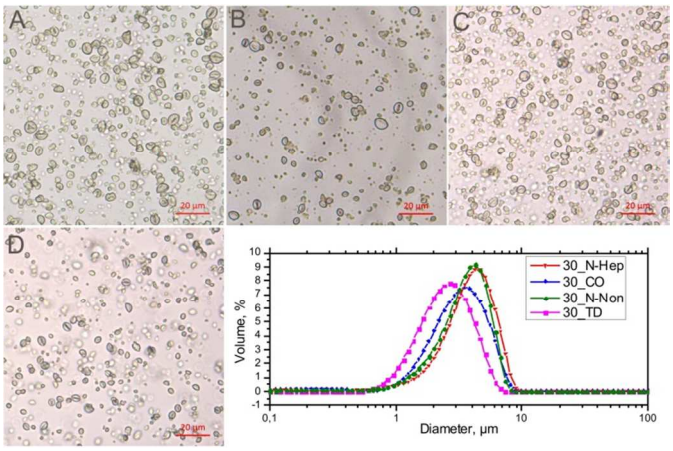

Fig. 3. Optical microscope images of particle suspensions after centrifugation: A)N-Hep, B) CO, C) N-Non and D) TD as well as their size distributions.

other absorption bands and, thus, can be easily identified.

Formation of the amide type bonds, which are absent in the original isocyanate prepolymer, can be followed by the emergence of the absorption bands at 1658 cm^{-1} (amide C=O stretching) and 1537 cm^{-1} (amide N-H bending). Appearance of these bands confirms the formation of a polymer of either polyurethane or -urea type. The peaks at 1598 and 1510 cm^{-1}, which are present in both isocyanate prepolymer and the polymerized material, can be attributed to the C-C stretching vibrations in the aromatic ring. The bands at 1312 and 1234 cm^{-1} can be attributed to the C-N stretching of aromatic secondary amine, however the peak at 1234 cm^{-1} can be also attributed to the carboxylic C-O stretching vibrations. The peaks between 1350 and 1480 cm^{-1} are due to the C-H bending in alkanes, while the ones between 2850 and 3000 cm^{-1} correspond to the alkane C-H stretching.

Polymerization reaction in all four types of particles was almost completed after 24 hours as confirmed by the almost complete disappearance of the band at 2275 cm^{-1} in FT-IR spectra. As expected, the spectra of the synthesized composite particles mainly differ from each other in the region corresponding the alkane C-H stretching (2850-3000 cm^{-1}) due to the different core materials used, while the fingerprint regions reflecting the structure of the polymer shell are almost identical. The bands between 2850 and 3000 cm^{-1} are matching those of individual core material.

Despite the similarity of the conditions used to prepare the dispersions, the size distribution of the particles in the resulting suspensions varies slightly. Fig. 3 shows the size distribution and the representative optical microscope images of the four types of particle suspensions.

Particle size distributions of the suspensions, where N-Hep (d_{max}=4,3 µm) and N-Non (d_{max}=4.2 µm) were used as the particle core material, are almost identical. The average particle size of the samples containing TD is smaller (d_{max}=2,7 µm), while the particles containing CO have slightly broader size distribution with the maximum (d_{max}=3,5 µm) shifted towards smaller sizes compared to N-Hep- and N-Non-containing ones. The difference can be explained by the differences in the oil phase compositions and viscosities (see SI for more details).

The shape of all types of particles is not spherical, resembling more the one of an air-balloon with some air being released. In the particular case, the "balloons" are filled with the liquid hydrocarbon instead of air. The non-sphericity of the resulting particles is probably due to the fact that formation of the partially solidified but still flexible polymeric shell happens faster than the release of the co-solvent (ethyl acetate). See fig. SI-2 for more details.

The shell has to adjust to the decreasing inner volume (due to the removal of the co-solvent) leading to the formation of the fold on one side.

The thermal stability of the resulting particles was analysed by TGA (fig. 4). Weight loss profile for the particles containing N-Hep exhibits a drop between 100 and 190°C. Between 190 and 290°C the weight of the sample remains almost unchanged, but decreases again between 290 and 320°C, after which it continues to decrease gradually. The particles containing higher hydrocarbons as the core material show higher thermal stability. For the N-Non-containing sample, the first drop of weight happens between 150 and 250°C, while the second, again, between 290 and 320°C followed by a gradual decrease. The particles containing CO are slightly more thermally stable than the ones containing N-Non: the first weight loss region can be found between 175 and 275°C, while the second one is slightly broader. The TD-containing particles do not exhibit almost any weight loss up to 290°C. Pure polyurethane starts to decompose at ~ 290°C.

The derivative curves of all samples exhibit two clear maxima. In accordance with the previously reported data [20], polyurethane thermal decomposition occurs in two steps, and the corresponding peaks in the weight-loss derivative graph are located at ca. 310 and 335°C. Similarly, all four samples with liquid cores exhibit a maximum at ~ 310°C. In the cases of He, CO and No the second maximum is rather small compared to

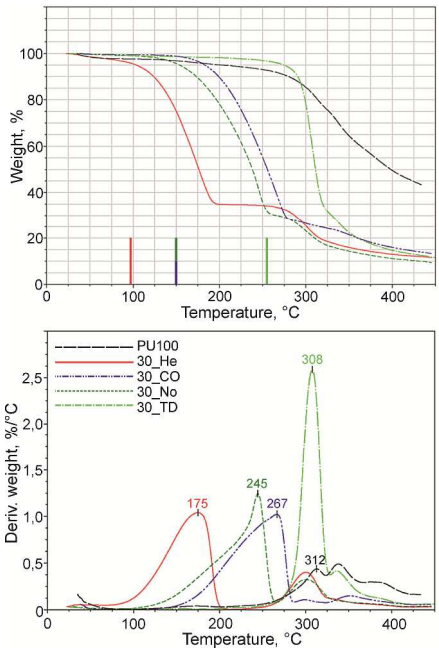

Fig. 4. Weight-loss curves and the first derivative of the weight-loss curves obtained for the particles with different core materials and for the pure shell material (PU100). The boiling points of individual core materials are marked by the lines of the corresponding colour.

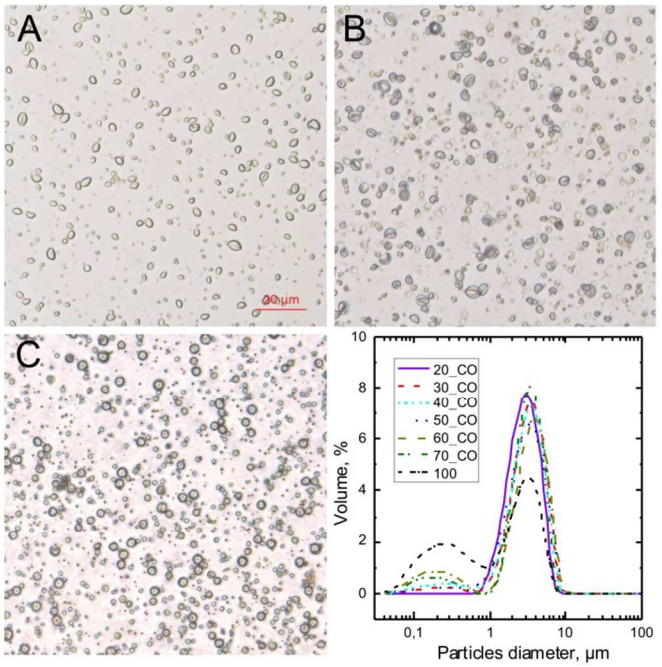

Fig. 5. Representative microscope images of the suspensions prepared at different shell thickness.: A) 20_CO, B) 50_CO, C) 100, and their particle size distributions.

the first one. The first maximum can be, thus, attributed to the evaporation of the core material (at 175, 245 and 267°C for He, No and CO, respectively), while the second one is due to the decomposition of polyurethane shell. In the case of TD the situation is rather different. It seems that evaporation of the liquid core happens simultaneously with the decomposition of polyurethane. An important observation is that the evaporation of the core material from the particles happens well above the boiling point of the individual hydrocarbon. Moreover, the higher the boiling point of the encapsulated material is, the higher is the thermal stability of the resulting core-shell particles. The difference in thermal stabilities of N-Non and CO containing particles correlates with the difference in the saturated vapour pressures of these compounds above 200°C). These results were not surprising, since few cases of the thermal stability improvement achieved by encapsulation have been already reported in the literature. For example, encapsulation of dicyclopentadiene in chitosan/urea-formaldehyde composite polymer (ca. 45 µm mean diameter, 40 wt.% solid content),[13] n-hexadecane in phenolic resin (6 µm mean diameter, ca. 50 % solid content),[21] IPDI in bi-layer polyurethane/poly(urea–formaldehyde) composite polymer (100 µm, 20 wt.% solid content)[15] led to a substantial improvement of the thermal stability of the core material. However, in some cases, encapsulation did not lead to any improvement of thermal stability.[12]

The release of the core material generally occurs in a certain temperature range. In order to extract quantitative information we will use the temperature corresponding to the position of the maximum in the weight-loss derivative graph as the characteristic value (T_c). At this temperature, the release of the liquid material happens with the highest velocity. In principle, one could also choose, for example, the 5 % weight loss (typically used in application studies) as the quantitative parameter for the thermal stability estimation. This is, however, not very convenient, since, as it will be shown below, the thermal stability of the core-shell particles is size-dependent. Therefore, discussing the results in terms of the weight loss begin would mean that the thermal stability of only a certain fraction of particles would be taken into account.

The TGA results allow us to conclude that the shell of the particles is able to withstand a certain inner pressure Pc corresponding to the temperature T_c. Each microparticle can be imagined as completely filled with liquid and having complex shape vessel of micron size, which is heated above the boiling point of the liquid. The pressure inside the vessel can be considered to be equal to the saturated vapour pressure of the liquid at the corresponding temperature (the legitimacy of the statement will be described in the discussion part). For hydrocarbons, the dependency of the saturated vapour pressure on temperature can be described by Antoine equation. Thus, the critical pressure (at which the mass loss happens at fastest) for each type of particles can be estimated and gives 6.3 Bars, 9.3 Bars, 7.4 Bars and 3 Bars for the particles filled with N-Hep, CO, N-Non and TD, respectively. In the case of TD, the critical pressure leading to the fast release of the core material was probably not reached, because the decomposition temperature of the shell material was reached before. The release of the liquid component basically took place because the walls of the

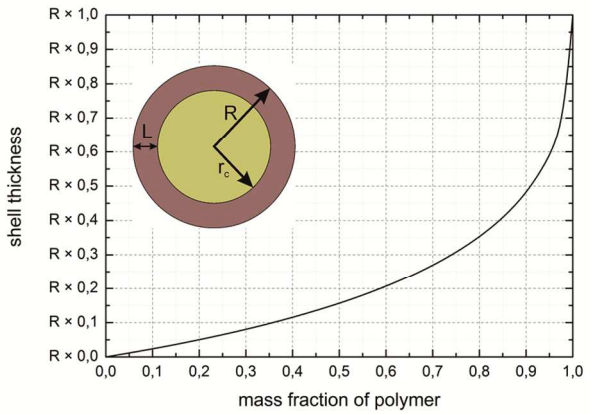

Fig. 6. Dependence of the particle shell thickness on the mass fraction of the shell material calculated using the densities of the core and the shell material equal to 0,8 g/cm3 and 1,2 g/cm3, respectively

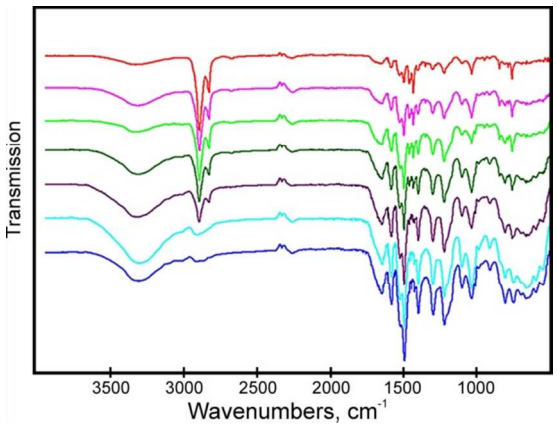

Fig. 7. FTIR spectra of the samples having different core/shell ratios. From top to down: CO_20, CO_30, CO_40, CO_50, CO_60,CO_70 and PU_100. The spectra are not normalized.

"vessel" started to degrade. The release mechanisms for the three other core materials will be discussed.

Shell thickness

In this set of experiments, we fixed the core material (CO) and varied the core-shell ratio. Seven samples with the isocyanate prepolymer content (calculated as X/(X+Z)×100%, see Table 1) of approximately 20, 30, 40, 50, 60, 70 and 100 wt. % wereprepared. Since the stirring speed during the emulsion preparation and, consequently, the average size of the resulting particles were nearly the same (fig. 5), it was the thickness of the polyurethane shell that varied in this experiment series.

The shell thickness (L) of a core-shell particle with the radius R can be expressed in terms of mass fraction of the core material (φ_c). The radius of the core (r_c) is related to the particle radius (R), mass fraction of the core (φ_c) and densities of the core (ρ_c) and the shell (ρ_s) materials according to the following formula:

$$r_c = R \times \sqrt[3]{\frac{\varphi_c \times \rho_s}{\varphi_c \times \rho_s + \rho_c - \varphi_c \times \rho_c}} \text{ (eq. 1), while}$$

$$\varphi_s + \varphi_c = 1 \text{ (eq. 2) and } L = R - r_c \text{ (eq. 3)}$$

Using the known densities of the oil phase (0,8 g/cm3) and polyurethane shell (1,2 g/cm3), the average shell thickness of the particles 20_CO sample (ca. 75 nm) is calculated (fig. 6) to be 5,36 times smaller than the average particle shell thickness in 70_CO sample (ca. 400 nm).

The representative microscope images of the particles with different core-shell ratio as well as their particle size distributions are shown in fig. 5. The shape of the particles is found to be dependent on the composition. Increase of the polymer content leads to the formation of the particles having more regular spherical shape. The particles of 20_CO are very far from being spherical, 50_CO particles are more spherical, while 100% polymer particles i.e. without a liquid core, are almost spherical.

Analysis of the FT-IR spectra (fig. 7) of the composite particles shows that the polymerization reaction in all the cases was nearly completed.

The change in the sample composition can be followed as well. Thus, the samples containing only 20 wt. % of the polymer had very pronounced absorption bands between 2850 and 3000 cm^{-1} due to the alkane C-H stretching. Reduction of the core content led to the decrease of the relative intensity of the C-H stretching bands and increase of the intensities of all the peaks corresponding to the polymer structure elements. In principle, FT-IR spectroscopy can be used for the quantitative analysis of the microparticles' composition.

The ratio of the intensities of the peaks (or their integrals) at 1510 and 2900 cm^{-1} (or the corresponding peak areas) can be used to plot a calibration curve, and the peak at ~1510 cm^{-1} can be used for the spectra normalization.

The results of the TGA investigations (fig. 8) indicated that the samples possess different thermal stabilities. Moreover, the composition of the samples can be easily determined from the corresponding m(T) graphs. Surprisingly, the solid content, which corresponds to the end of the first weight loss step, in all the samples was found to be close to the initial amount (±3 wt.%) of the isocyanate prepolymer (calculated as X/(X+Z)×100%, see Table 1). Since the polymer is formed by the polyaddition reaction between isocyanate and glycerol, the content of the polymer was expected to be higher than the initial amount of the isocyanate prepolymer. At the same time the reaction of isocyanate with water also takes place. This reaction leads first to the formation of an unstable intermediate, which decomposes to give carbon dioxide and an amine, which, in turn, can further participate in the polymer network formation. Taking into account that all isocyanate groups have reacted (as observed by FT-IR) and assuming that all the hydroxyls from glycerol molecules attached to the polymer matrix have reacted as well (which is, in fact, not very realistic), one could estimate the minimum content of the urea linkages as 43 % (43 out of 100 linkages are of urea type). Taking into account that reaction of the second and, especially, the third hydroxyl group of the glycerol is sterically hindered, some hydroxyls probably stay unreacted, which means that the content of urea linkages is probably even higher.

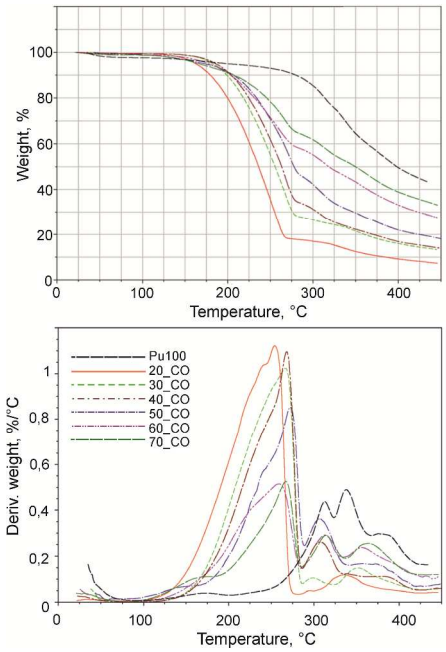

Fig. 8. Weight loss profiles and their deriavatives for microparticles having the same size but different composition (shell thickness).

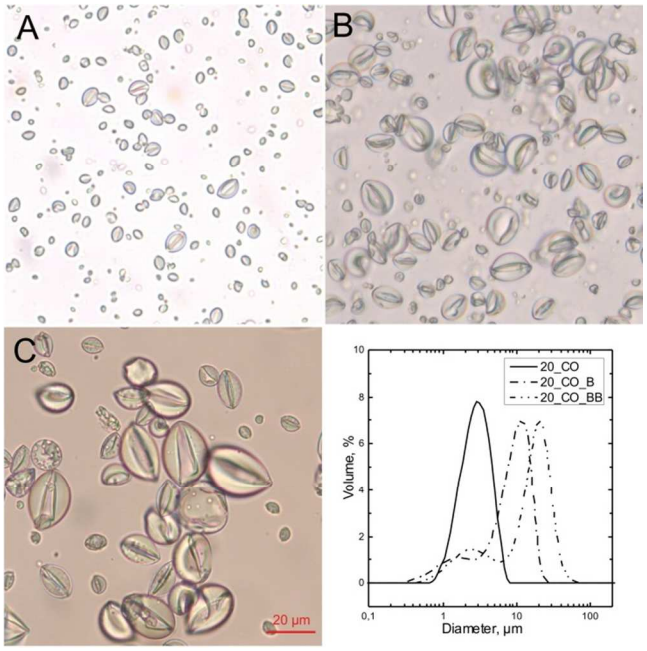

Fig. 9. Optical microscope images of the suspensions of the particles with the same composition but different size: 20_CO (A), 20_CO_B (B) and 20_CO_BB (C).

The thermal stability of the samples estimated in terms of the first maximum position on the weight loss derivative curve is only slightly influenced by the change of the composition. The positions of the maxima vary within 15°C, but no clear trend can be observed. This was a quite surprising finding taking into account that the particle shell thickness was varied in a broad range (from 75 to 400 nm, Fig. 6).

Particle size

In this experiment series, the stirring speed of the high shear mixer during the emulsion preparation was varied, while the composition of the oil phase was kept constant (CO, 20 wt. % solid content). The decrease of the stirring speed led to the formation of bigger particles (fig. 9). Thus, the average particle size distributions of particles prepared at 3000 and 5000 rpm are bimodal with the positions of the main maximums at 20,7 µm and 11,8 µm, respectively. One has to consider that the bigger particles also have thicker shells. The shell thickness is proportional to the particle radius if the composition is fixed. The extent of the polymerization reaction in the particle shell is found to depend on the particle size (fig. 10). Even after 3 days of reaction, isocyanate peak is much more pronounced in the

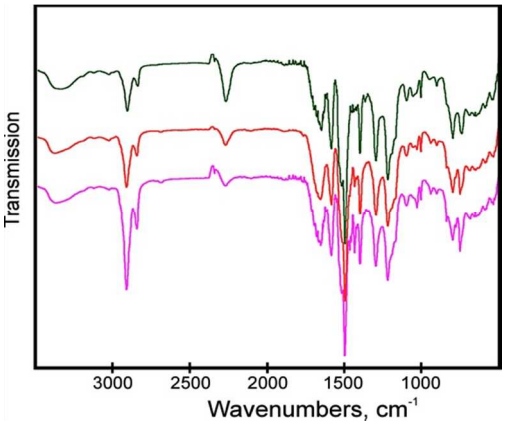

Fig. 10. FT-IR spectra of particles having the same composition but different sizes. From top to down: 20_CO_BB, 20_CO_B, 20_CO. The spectra are normalized to the peak corresponding to the C-C stretching in the benzene ring (~1510 cm^{-1}).

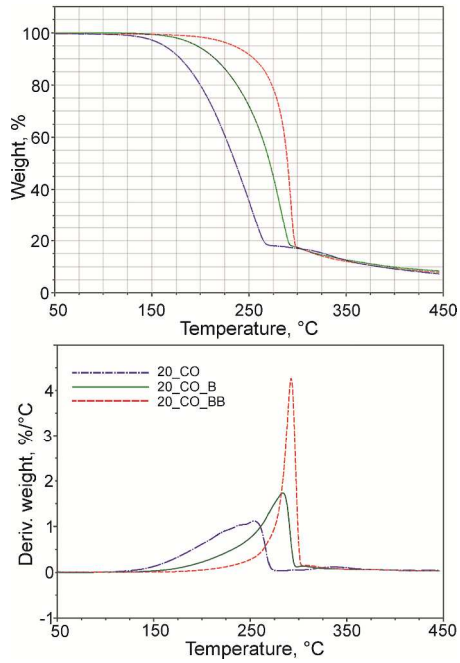

Fig. 11. Mass loss profiles (left) and their deriavatives (right) for microparticles having the same composition but different sizes.

case of bigger particles if compared to the smaller ones (note that the FT-IR spectra in fig. 10 are normalized to the ~1510 cm-1 band). In spite of the fact that the particles had the same composition, the relative intensity of the bands between 2850 and 3000 cm^{-1} (corresponding to the hydrocarbon core material) is smaller in the case of bigger particles. See the explanation of the phenomenon in the SI.

In spite of the fact that isocyanate conversion in bigger particles was smaller, their thermal stability was substantially higher. Thus, the fastest weight loss for smaller particles is observed at 254°C, for bigger ones – at 284°C, while for the biggest ones – at 292°C. The critical pressures corresponding to the maxima of the weight loss derivative curves are: 7.6, 11.9 and 13.2 Bars for 20_CO, 20_CO_B and 20_CO_BB, respectively.

Discussion:

Obtained results can be summarized as following:

- The higher the boiling point of the core material, the higher the thermal stability of the composite particles.
- Fastest release of the core material from the particles occurs well above the boiling temperature of the core material. Notice that due to the small volume of the TGA samples (≤ 7 mg), evaporation of the comparable amount of a free (non-encapsulated) hydrocarbon happens before reaching the boiling point.
- The thickness of the particle shell almost does not influence the thermal stability (defined as T_c) of the particles.
- Size matters: bigger particles are considerably more stable than the smaller ones with the same composition.

Non-sphericity of the particles as well as their broad size distributions complicate the analysis of the results, some information can be extracted, nevertheless.

Each microparticle can be imagined as completely filled with a liquid and having complex shape vessel. Theoretically, four different mechanisms responsible for the release of the liquid from the vessel can be considered:

(1) "Explosion" of the vessel due to the inner gas pressure equal to the saturated vapour pressure of the enclosed liquid (occurs above the boiling point of the liquid).

(2) Rupture of the vessel's wall due to the inner pressure caused by the thermal expansion of the liquid (thermal expansion of the wall material is smaller). In this case the rupture can happen below the boiling point of the liquid.

(3) Diffusion of the liquid through the vessel's wall, without damaging the latter.

(4) Thermal decomposition of the vessel's wall and subsequent release of the liquid.

In case of TD-filled microparticles, the decomposition mechanism corresponds to the thermal decomposition of the shell. In all other cases, the weight loss occurs before the wall material starts to degrade. Consequently, the degradation occurs by either of three other mechanisms.

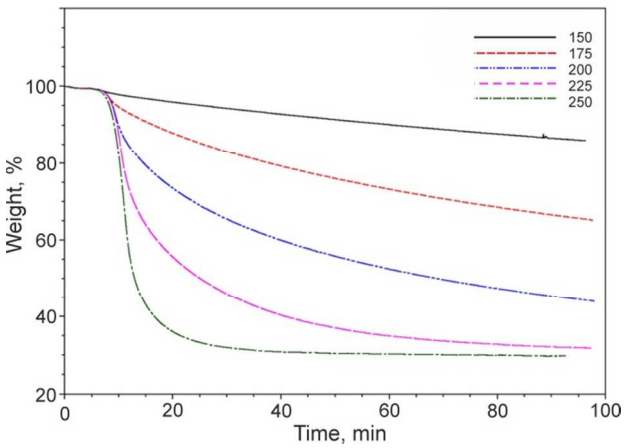

Fig. 12. Weight vs. time profiles of CO_30 sample heated to and held at a certain temperature for 90 minutes. The temperatures are 150, 175, 200, 225 and 250°C.

The first two mechanisms are the examples of a catastrophic event, which assumes that once the critical pressure (limited by the mechanical strength of the wall material) is reached, immediate release of the entire volume of a core material takes place (assuming that evaporation of the liquid through a defect in the shell at the temperature corresponding to the limiting pressure is happening very fast). Among the three, the third mechanism is the only one that implies gradual release of the core material with time.

In order to be able to distinguish between the first three mechanisms, an additional experiment, which reflects the kinetics of the process, has been performed. For that, one of the samples (30_CO) was heated (20 K/min) to predetermined temperatures (150, 175, 200, 225 and 250°C) and held at each temperature for 90 minutes. The change of the mass with time is shown in fig. 12.

As one can see, the release of the core material happens gradually, and the velocity of the process depends on the temperature.

It is clear now that the release could happen neither by the first nor by the second suggested mechanisms, because otherwise, the release would have taken place in a step-like manner. All particles that have reached the mechanical stability limit (which should depend on the radius and the wall thickness) after reaching the corresponding temperature would release their entire core content. The latter would be immediately evaporated (evaporation of a drop of CO at 150°C happens within one minute) and no further change of mass with time would be observed.

Thus, one has to conclude that the release happens according to the mechanism 3: diffusion of the core material through the particle shell. The shell of each particle can be considered as a membrane, through which the core material "pervaporates".

The surface of the membrane is equal to the surface area of the particle. The pressure inside each particle can be considered to be equal to the saturated vapor pressure of the core material at the corresponding temperature. At constant temperature, the

pressure is constant until most of the liquid content has diffused out of the particle.

Pervaporation process can be described by Graham' solution diffusion model. It involves the dissolution of penetrant molecules in the polymer membrane followed by the diffusion of the dissolved species. In the steady state conditions approximation (implies that diffusant concentrations remain constant at all points on each side or surface of a plastic membrane), the whole process can be described by a simple formula:[22, 23]

$$J = -\frac{dm/dt}{A} = \frac{D \times S \times (P_2 - P_1)}{L} \text{ (eq.4),}$$

which is derived from Fick's first law:

$$J = -D \times \frac{dC}{dx} \text{ (eq.5)}$$

and Henri's law, which postulates that the concentration of the gas in the membrane is directly proportional to the applied gas pressure:

$$C = P \times S \text{ (eq.6),}$$

where J is the diffusion Flux, m is the mass (of the sample in TGA), t is the time, A is the area available for the pervaporation, D is the diffusion coefficient of the diffusant (core material) in the plastic membrane (particle shell), S is the solubility coefficient of the diffusant in the membrane, C is the concentration of the diffusing substance, x is the space coordinate measured normal to the section, L is the membrane thickness and P is the pressure on either side of the membrane.

If equation 2 and the steady state conditions approximation are valid, one would normally expect linear dependency of the weight loss on time, which is in fact not observed. The solution of this apparent contradiction is in consideration of the broad particle size distribution of the samples. Thus, it can be shown that the release of the core material from the smaller particles happens faster than from the bigger ones. This is due to the fact that smaller particles have thinner shells (shell thickness is proportional to the radius) and higher area available for the pervaporation (surface area available for the pervaporation is inversely proportional to the radius). The surface area of each particle is proportional to the particle radius squared R^2 (for spherical particles). At the same time, the number of particles is inversely proportional to each particle volume, which is, in turn, proportional to R^3. As the result, the total area available for the pervaporation is inversely proportional to the particle radius (in each fraction with the radius R_i). Thus, if the composition of the particles is fixed and the influence of both, membrane thickness and area, are considered, the following relation is valid:

$$-\frac{dm}{dt} \propto \frac{1}{R^2} \text{ (eq. 7)}$$

Thus, it can be concluded that non-linear dependency of the weight loss on time comes from the fact that the smaller particles release the core material faster than the bigger ones. With time, all the available core material from the smaller particles is released leading to the decrease of the dm/dt slope. In order to prove that the mass loss profile can indeed have the observed non-linear shape solely due to the broad particle size distribution, we have performed a simple simulation (see SI), which confirms the assumption. Thereby, the contradiction is solved.

The results of each experimental series can be qualitatively explained within the same paradigm. One important point that the reader has to keep in mind is that all the measurements that have been performed here were out of equilibrium. The samples were typically heated with 10 K/min speed, which led to the increase of the inner pressure. At the beginning of the heating process, the diffusion coefficients of hydrocarbons in polyurethane are relatively low. Therefore, almost no weight loss can be detected. Once the temperature reaches and exceeds the boiling point of the core component, the driving force that pushes the core component through the membrane starts to act. Though the heating is performed in the linear mode, the inner pressure increases exponentially (according to the Antoine equation). At the same time, temperature increase leads to the fast increase of the diffusion coefficient of the core material in the polymer membrane (also exponentially, according to Arrhenius' equation). According to this, the flux increases very fast with the increase of temperature.

In the first experimental series, the core material has been varied. The estimation of the critical pressure for each type of particles gave 6.3 Bars, 9.3 Bars and 7.4 Bars for the particles filled with N-Hep, CO and N-Non, respectively. No trend in the critical pressure (neither related to the molar mass nor to the boiling point of the core component) could be identified. The difference in the P_c values for the different components can probably be explained by the difference in their D(T) dependencies. The critical pressure is thus hard to predict, since very few empirical data on the D(T) is available.

In the second experimental series, the size of the particles was fixed, while the shell thickness was varied. Again, no trend has been recognized. This was very surprising, since flux is inversely proportional to the particles' shell thickness. One could assume that the dependency on the shell thickness is (almost) not detectable, because the dependency of the pervaporation speed on the shell thickness is linear, while its dependency on temperature is exponential. In such a manner, the 5-fold increase in shell thickness can probably be compensated by 5-fold increase of flux within 10°C (consider that the sample is constantly heated with 10°C per minute).

In order to understand the results of the third experimental series (fixed composition, varied size) one has to keep in mind that the pervaporation speed is inversely proportional to the R^2. The difference in the average particle size in the three batches of particles was so big, that it probably could not be completely compensated by the increase of the diffusion coefficient and pressure with temperature. Therefore, the dependency on size could be observed.

Quantitative validation of the concept presented here will require estimation of the diffusion coefficients for each component as well as their dependency on temperature. For this

purpose, thorough studies on the kinetics of the weight loss have to be performed. Unfortunately, this is not possible within the scope of this manuscript.

Conclusions

Herein, we have shown that enclosing a liquid in a polymeric shell can decrease its volatility substantially. The process of the liquid evaporation in this case is limited by the diffusion of the liquid through the each particle's shell. It turns out that the observed in a typical TGA measurement stability of the microparticles is dictated by their size (if the composition is fixed), but almost does not depend on the shell thickness (if the size of the particles is fixed). As far as we know, this effect has been observed for the first time. Despite their small size (≤70 μm), the microparticles are able to withstand surprisingly high inner pressure (up to 13 bar) without being mechanically ruptured.

These findings are obviously of great practical importance for the development of more thermally stable polymer composite microparticles. The obtained knowledge is also significant for the development of new thermally triggered release systems. With the mechanism of the release in mind, one could think of the new applications, for which e.g. preferential release of one specific component of a mixture at a certain temperature would be desirable.

The obtained knowledge is also potentially useful for the better understanding of the high temperature processes aimed at production of materials with complex architecture at nano and micro scale. Synthesis of such materials (e.g. carbonization) normally goes through several decomposition-reaction-precipitation steps. By-products, formed at one of the synthesis steps, can be eventually trapped inside the precipitated structures. The mechanism of the by-products release can have great influence on the final morphology of the synthetic product. Thus, one could expect that the "explosion" mechanism would lead to the formation of the structures with the open cell morphology and high available surface area. Recognized in this paper "diffusion" mechanism would probably rather favour formation of denser structures with closed cell morphologies.

Acknowledgements

The authors are very happy to express their gratitude to Monika Jobmann and Dr. Dariya Dontsova for their invaluable help and support during the manuscript preparation. We would also like to thank Malies Walter for the particle size distribution measurements.

Notes and references

[a] Fraunhofer Institute for applied polymer research, Geiselbergstr. 69, 14476, Potsdam-Golm, Germany.
e-mail: alexandra.latnikova@iap.fraunhofer.de

† Electronic Supplementary Information (ESI) available: [details of any supplementary information available should be included here]. See DOI: 10.1039/b000000x/

1 S. J. Garcia, H. R. Fischer and S. van der Zwaag, *Progress in Organic Coatings*, 2011, **72**, 211-221.
2 M. R. Kessler, N. R. Sottos and S. R. White, *Composites Part a-Applied Science and Manufacturing*, 2003, **34**, 743-753.
3 K. S. Toohey, N. R. Sottos, J. A. Lewis, J. S. Moore and S. R. White, *Nature Materials*, 2007, **6**, 581-585.
4 Q. B. Guo, K. T. Lau, B. F. Zheng, M. Z. Rong and M. Q. Zhang, *Macromolecular Materials and Engineering*, 2009, **294**, 20-24.
5 M. A. Trojer, L. Nordstierna, J. Bergek, H. Blanck, K. Holmberg and M. Nydén, *Advances in Colloid and Interface Science*, doi:10.1016/j.cis.2014.06.003.
6 V. V. Tyagi, S. C. Kaushik, S. K. Tyagi and T. Akiyama, *Renewable & Sustainable Energy Reviews*, 2011, **15**, 1373-1391.
7 P. Soon-Shiong, N. P. Desai, P. A. Sandford, R. A. Heintz and S. Sojomihardjo, US5705270 A, 1998.
8 S. Cui, F. Ya-Qing, Z. Bao, L. Xiang-Gao, S. Ji-Zhou, H. Jing-Jing and C. Xu, *Optical Materials*, 2013, **35**, 1410-1417.
9 Y. Shibahashi and A. Sukai, JP2002129030-A, 2002.
10 N. Yamaguchi, K. Sano and H. Inoue, JP2008296971-A, 2005.
11 Q. Song, Y. Li, J. Xing, J. Y. Hu and Y. Marcus, *Polymer*, 2007, **48**, 3317-3323.
12 L. Bayés-García, L. Ventolà, R. Cordobilla, R. Benages, T. Calvet and M. A. Cuevas-Diarte, *Solar Energy Materials and Solar Cells*, 2010, **94**, 1235-1240.
13 R. Wang, H. Hu, X. He, W. Liu, H. Li, Q. Guo and L. Yuan, *Journal of Applied Polymer Science*, 2011, **121**, 2202-2212.
14 C. Gong, H. Zhang and X. Wang, *Iranian Polymer Journal*, 2009, **18**, 501-512.
15 B. Di Credico, M. Levi and S. Turri, *European Polymer Journal*, 2013, **49**, 2467-2476.
16 X. Qiu, L. Lu, J. Wang, G. Tang and G. Song, *Solar Energy Materials and Solar Cells*, 2014, **128**, 102-111.
17 L. Chen, L.-Q. Zhang, R.-F. Tang and Y.-L. Lu, J*ournal of Applied Polymer Science*, 2012, **124**, 689-698.
18 L. Yuan, G.-Z. Liang, J.-Q. Xie, L. Li and J. Guo, *J Mater Sci*, 2007, **42**, 4390-4397.
19 S. K. Yadav, K. C. Khilar and A. K. Suresh, *Aiche Journal*, 1996, **42**, 2616-2626.
20 S. Foti, P. Maravigna and G. Montaudo, *Journal of Polymer Science Part a-Polymer Chemistry*, 1981, **19**, 1679-1687.
21 Y. Jiang, D. Wang and T. Zhao, *Journal of Applied Polymer Science*, 2007, **104**, 2799-2806.
22 A. F. Ismail, T. D. Kusworo, A. Mustafa and H. Hasbullah, *Proceedings of the 2005 Regional Conference on Engineering Education*, Malaysia, 2005.
23 E. Drioli and L. Giorno, *Comprehensive Membrane Science and Engineering*, Elsevier Science, 2010.

